A promising composite anode for solid oxide fuel cells: $Sr_2FeMo_{0.65}Ni_{0.35}O_{6-\delta}$-$Gd_{0.1}Ce_{0.9}O_{2-\delta}$

Yanru Yang[a], Zhibin Yang[a*], Yu Chen[b*], Fanglin Chen[c], Suping Peng[a]

[a] Union Research Center of Fuel Cell, China University of Mining and Technology, Beijing, China

[b] School of Materials Science and Engineering, Georgia Institute of Technology, Atlanta, USA

[c] Department of Mechanical Engineering, University of South Carolina, Columbia, USA

Abstract

Coking on the conventional Ni-based anode is a grand challenge for direct hydrocarbon solid oxide fuel cells. In this work, a new type of coking-tolerant composite anode material, with a composition of $Sr_2FeMo_{0.65}Ni_{0.35}O_{6-\delta}$-$Gd_{0.1}Ce_{0.9}O_{2-\delta}$, has been identified and evaluated on $Y_{0.08}Zr_{0.92}O_{1.96}$ electrolyte-supported cells. The X-ray diffraction analysis indicates that the crystal structure of $Sr_2FeMo_{0.65}Ni_{0.35}O_{6-\delta}$ is relatively stable in wet air, while active nanoparticles of $FeNi_3$ are in situ exsolved from the parent perovskite oxides in pure hydrogen. A peak power density of 439 mW cm^{-2} at 850 ^oC is achieved from the cell with $Sr_2FeMo_{0.65}Ni_{0.35}O_{6-\delta}$ anode when fueled by hydrogen. More importantly, addition of $Gd_{0.1}Ce_{0.9}O_{2-\delta}$ in the anode can further improve the performance and stability. The cell with $Sr_2FeMo_{0.65}Ni_{0.35}O_{6-\delta}$-$Gd_{0.1}Ce_{0.9}O_{2-\delta}$ composite anode achieves a maximum power density of 551, 476 and 392 mW cm^{-2} at 850 ^oC when the anode is fueled by hydrogen, syngas and methane, respectively. The cell has shown negligible degradation for 210 hs in syngas and 600 hs in methane fuel, indicating that the $Sr_2FeMo_{0.65}Ni_{0.35}O_{6-\delta}$-$Gd_{0.1}Ce_{0.9}O_{2-\delta}$ is a promising anode for solid oxide fuel cells.

Key words: Solid oxide fuel cells; ceramic anode; coking tolerance

* E-mail: yangzhibin0001@163.com; yu.chen@mse.gatech.edu

1. Introduction

Increased consumption of fossil energy in the past several decades has resulted in serious environmental concerns. As an efficient and environment-benign approach to produce electricity, fuel cell has attracted extensive research interests in recent years. Among the different types of fuel cells, solid oxide fuel cell (SOFC) possesses the unique advantages of all solid state cell components and ability of direct utilization of hydrocarbon-based fuels [1, 2]. However, the traditional Ni-cermet SOFC anodes are unstable for direct oxidation of natural gas or other hydrocarbon fuels since the Ni surface can be severely deactivated by carbon deposition (coking), unless reforming of the fuel stream is realized through supply of significant amount of steam or air [3, 4].Therefore, many efforts have been devoted to explore alternative SOFC anode materials with coking resistance for direct electrochemical oxidation of hydrocarbon fuels [5-7], which would be of high significance for eliminating the fuel reforming process, improving the SOFC system efficient and reducing the cost. Among the different alternative SOFC anode materials reported, perovskite based oxides such as $La_{0.75}Sr_{0.25}Cr_{0.5}Mn_{0.5}O_{3-\delta}$ (LSCM) [8], La-and Y-doped $SrTiO_3$ [9], $Sr_2MgMoO_{6-\delta}$ [10], and $Sr_2Fe_{1.5}Mo_{0.5}O_{6-\delta}$ [11] have been extensively explored. However, either the conductivity or the catalytic activity (towards fuel oxidation) of those perovskite materials is not satisfactory, leading to lower cell power densities than that of Ni-based anodes.

One successful strategy in recent years is to improve the performance of perovskite ceramic anodes by introduction of nanoscale metallic catalyst particles on the parent perovskite surfaces. There have been a series of catalyst particles being produced by infiltration process [12, 13]. However, repeated infiltration and firing are complex and time-consuming, causing the growth of nanoparticles. On the other hand, in-situ growth of reducible alloy from ceramic parent oxides has

been demonstrated to be an effective process to generate uniformly dispersed electro-catalytic nanoparticles on the ceramic anode surface [14]. In our prior work, perovskite based anode materials of $Pr_{0.4}Sr_{0.6}Co_{0.2}Fe_{0.7}Nb_{0.1}O_{3-\delta}$ and $La_{0.4}Sr_{0.6}Co_{0.2}Fe_{0.7}Nb_{0.1}O_{3-\delta}$ have been developed, which can in situ form Co−Fe alloy nanoparticles [15, 16]; these nanoparticles significantly improve the activity and durability of the SOFC anodes when operating with hydrocarbon fuels.

Recent study has also demonstrated that Ni−Fe alloy nanoparticles, formed on the surface of $Sr_2FeMo_{1-x}Ni_xO_{6-\delta}$ (SFMN) anodes via in situ reduction, improved the electronic conductivity of electrode materials. The total electrical conductivity can be reached 55.4 S cm^{-1} at 800 °C [17]. However, the ionic conductivity of SFMN may not be adequate. Ceria-based oxide has been typically used to further increase the electrode ionic conductivity and extend surface reaction sites in SOFC anodes, especially for SOFCs using hydrocarbon fuels [18]. Further, the coefficient of thermal expansion of $Sr_2Fe_{1.5-x}Ni_xMo_{0.5}O_{6-\delta}$ increases from 15.6×10^{-6} K^{-1} to 18.1×10^{-6} K^{-1} with x from 0.05 to 0.4, which are little higher than that of YSZ (10.8×10^{-6} K^{-1}) [19]. Therefore, addition of GDC is also necessary to improve adhesion between the electrolyte and the electrode.

Here, we report a composite of SFMN and GDC as potential anode materials for SOFCs operating in carbon-containing fuels such as syngas and methane. The in situ exsolved metallic nanoparticles from the SFMN-GDC composite has demonstrated promising fuel oxidation activity and coking resistance. More importantly, the performance and stability is improved significantly by addition of GDC.

2. Experimental

The perovskite $Sr_2FeMo_{0.65}Ni_{0.35}O_{6-\delta}$ (SFMN) was prepared by a conventional solid-state reaction method. The high purity precursors powders including $SrCO_3$, Fe_2O_3, $(NH_3)_6Mo_7O_{24}\bullet4H_2O$,

$Ni(NO_3)_2$•$6H_2O$ were mixed at the stoichiometric ratios. The mixtures were ball-milled in ethyl-alcohol with zirconia balls for 48 hs and then dried in oven at 70 °C for 24 hs. The precursor were fired at 1100 °C for 10 hs in air to obtain the perovskite phase, and then reduced in pure H_2 at 850 °C for 10 hs for X-ray diffraction (XRD) measurements. $Gd_{0.1}Ce_{0.9}O_{2-\delta}$ (GDC) powders were purchased from Ningbo SOFCMAN Energy Technology Co. The SFMN-GDC (mass ratio of 5:5) slurry was screen-printed on the surface of the GDC/YSZ/GDC electrolyte, which were purchased from Huaqing Company (Kunshan, China), followed by calcining at 1150 °C for 2 hs. An electrode ink consisting of $La_{0.6}Sr_{0.4}Co_{0.2}Fe_{0.8}O_{3-\delta}$（LSCF）was applied as a cathode using screen-printing and fired at 1000 °C for 2 hs. The active area of both the anode and cathode is approximately 0.5 cm^2, and the thickness of electrodes is about 50 μm. The thickness of the YSZ electrolyte films is about 170 μm, and GDC buffer layer is about 10 μm. The single-cell performance was evaluated with the cells with a configuration of SFMN-GDC‖GDC/YSZ/GDC‖LSCF.

The crystal structure of different powders after annealing was examined by XRD technique (PANalytical X'Pert PRO, Netherlands), with a scanning step of 0.02° in the 2θ range of 10-90°. The morphology of the electrodes was characterized by scanning electron microscopy (SEM, FEI Quanta 200). The electrochemical characterizations (IV curves and electrochemical impedance spectra) of single cells were typically measured with IM6 & Zennium Electrochemical Workstations. The frequency of electrochemical impedance ranges from 0.1 Hz to 1 MHz. Before testing, the cells were first reduced in H_2 at 850 °C for 2 hs which were sealed on the alumina testing apparatus with a ceramic bond. Then the electrochemical measurements were evaluated in the temperature range of 700 to 850 °C, using H_2, syngas (H_2-CO, 1:1) or CH_4 humidified with 3%H_2O as fuel.

3. Results and discussion

3.1 XRD analyses

The X-ray diffraction (XRD) patterns of as-prepared and reduced SFMN (in pure H_2 for 10 hs powders at 850 ^oC) were compared in Fig. 1(a). Before reduction, the SFMN powder exhibited a tetragonal structure (I4/m, JCPDS 15-0601) with strong sharp diffraction peaks. The two weak peaks of around 19 and 38° indicated the double perovskite structure of the SFMN, and lattice parameters for the SFNM material can be refined as a=b=5.54, c=7.87. No obvious secondary phases were observable, indicating that Ni was fully incorporated into the perovskite structure.

As shown in Fig. 1a, the perovskite structure of reduced-SFMN was still maintained after reduction in pure H_2 at 850 ^oC for 10 hs (SFMN-reduced). The main peaks shift to lower angles, an indication of a lattice expansion after reduction, most-likely caused by oxygen loss. However, new peaks (of ~43.8 ^{o}) were detected, which were indexed well with $FeNi_3$ alloy structure (JCPDS 65-3244) and $Sr_3FeMoO_{7-\delta}$ (JCPDS 52-1715) [17]. $FeNi_3$ alloy phase was formed by exsolution of the parental perovskite phase, and the phase transformation generally occurred on the perovskite grain surface, which will potentially enhance the electrochemical performance of materials as SOFC anodes.

Generally, SFM-based perovskite materals will react with YSZ electrolyte, with the formation of $SrMoO_4$ and $SrZrO_3$ as main reaction products[20]. Therefore, GDC interlayer was deposited between electrodes and YSZ in this work. Shown in Fig.1(b) is the room temperature XRD patterns for GDC, SFMN as well as SFMN-GDC pellets sintered at 1200 ^oC for 5 hs in air. No impurity phases can be observable in the XRD pattern of the high temperature-treated SFMN-GDC mixed powders, compared to the XRD patterns of pure GDC and SFMN powders. These results indicated that SFMN and GDC were chemically compatible.

3.2 Microstructure Characterization of Cells

Fig.2(a) showed a cross-sectional scanning electron microscopic (SEM) image of the SFMN-GDC‖GDC/YSZ/GDC‖LSCF cell, the SFMN-GDC anode and the electrolyte adhered very well, and the electrode thickness of SFMN-GDC was about 50 μm. The thickness of the YSZ electrolyte films was about 170 μm and GDC buffer layer was about 10 μm. A detailed SEM view of the as-prepared SFMN-GDC anode (Fig.2b) showed porous structure with homogeneous particle size distribution and a clean smooth grain surface.

After reduction in pure H_2 at 850 ºC for 2 hs, some nanosized particles with diameters of 30–60 nm precipitated out, as shown in Fig.2c. The nano particles are most likely Fe-Ni alloy, indicated by XRD analyses. The nanosized particles are almost stable after three redox cycles at 800 ºC, an average particle size of ~60 nm, as shown in Fig.2d. For further comparison, the microstructure of SFM-GDC anode treated by similar reduction process was also shown in Fig.2f; the results showed that no obviously nanoparticles were observed.

3.3 Cell Performance in H_2

Shown in Fig.3a is the EIS data measured at different temperatures for the SFMN-GDC‖GDC/YSZ/GDC‖LSCF cell. Fig. 3b presents an example of EIS fitting from the cell with SFMN-GDC and SFMN anode, tested at 850 ºC using H_2 as fuel. The impedance spectra data for both anodes were fitted using the equivalent circuit model consisting of an inductor, a resistive element, and three R-CPE elements, which was similar as used in the reference [21]. The fitting with three R-CPE elements matched well with the experimental data. The ohmic resistances (R_Ω) of SFMN and SFMN-GDC anodes were ~ 0.47 and 0.45 Ω cm^2, respectively. The R_Ω corresponds to the ohmic resistances, involving ionic resistance of the electrolyte and the contact resistance

associated with interfaces. The slightly difference is within the experimental error.

The impedance spectra in Fig.3b showed an overlay of likely three depressed semicircles. The high-frequency responses in Fig.3b, which did not vary with above two type fuel cell anodes, can be attributed to the cathode. In the cell with SFMN-GDC anode, semicircles of the medium-and low-frequency were much smaller than those of cell with SFMN anode; hence the difference must be associated with anode processes [22]. Take the impedance spectra at 850 ^{o}C as an example, R_{LF} of the SFMN-GDC cell (0.072Ωcm^2) was less than half that of the SFMN cell (~0.287Ω cm^2). The difference may owe to the increased rate of ionic diffusion or adsorption process, especially the extended three-phase boundary. Further, ionic conduction may have been increased by addition of GDC, which may occur in the process associated with middle frequency range.

Overall, the total impedance of cell with SFMN-GDC anode was much smaller than that with SFMN anode due to the addition of GDC. Although SFMN was a mixed conductor of oxide-ion and electron hole with high electrical conductivity, it showed higher impedance value due possibly to its low ionic conductivity. With the addition of GDC with SFMN to form a composite anode, the mixed conductivity and catalytic activity of the composite anode is increased, as well proved in the literature [23, 24].

Fig. 4a showed the typical current density-voltage-power density curves of SFMN-GDC‖GDC/YSZ/GDC‖LSCF single cell with hydrogen as fuel and ambient air as oxidant. The open-circuit voltage (OCV) values were about 1.09 V at 850 ^{o}C, close to the Nernst potential, indicating a dense electrolyte and a good sealing of the tested cells. Maximum power densities of 551, 475, 366 and 271 mW cm^{-2} can be achieved at 850, 800, 750 and 700 ^{o}C, respectively. The performance is higher than the electrolyte supported cell with LSCFN-GDC anode [25]. One

possible reason is the high catalytic activity of $FeNi_3$ nanoparticles toward H_2 oxidation. The $FeNi_3$ nanoparticles were in situ exsolved from the SFMN ceramic backbone, and homogeneously coated on the substrate surface, which can effectively accelerate the electrode reaction processes. Additionally, compared with the SFMN‖GDC/YSZ/GDC‖LSCF cell with SFMN anodes, the maximum power densities in H_2 increased from 439 mW cm^{-2} up to 551 mW cm^{-2} at 850 ℃. The improved performance was mainly attributed to the addition of GDC, which can provide the ionic conduction path, extend the reaction zone, and thus reducing the polarization resistance, as similar shown in Fig. 3b. Moreover, the SFMN-GDC ‖ GDC/YSZ/GDC ‖ LSCF cell also showed a stable power output at 850 °C under a constant current density of 0.45 A cm^{-2}, as demonstrated in Fig.4b, indicating that the SFMN-GDC anode have excellent electrochemical performance and good short-term structural stability.

3.4 Cell Performance in CO-H_2

The performance of single cells has also evaluated in syngas (H_2:CO=1:1). Shown in Fig.5 are the I-V-P curves of cells with a configuration of SFMN-GDC ‖ GDC/YSZ/GDC ‖ LSCF, using air as oxidant and CO-H_2 (1:1) as fuel at 700-850 ºC. The peak power densities of the cell are 476, 390, 294 and 199 mW cm^{-2} fueled by a mixture of H_2-CO at temperatures of 850 ℃, 800 ℃, 750 ℃ and 700 ℃ respectively, as shown in Fig. 5a, suggesting that SFMN-GDC have good catalytic activity to syngas oxidation.

However, the peak power density of the cell is 551 mWcm^{-2}, which is higher than that 436 mW cm^{-2} of cell when fueled by pure CO only at the same operating temperature of 850 ℃. These results indicated that the SFMN-GDC composite anode had better electrocatalytic activity towards H_2 oxidation than CO fuel. The area specific resistance (ASR) was fitted using the equivalent circuit

model ($LRs(RHF)_1(RMF)_2(RLF)_3$), as shown in the Fig. 5b. The total polarization resistances were fitted to be 0.128 Ω cm^2 in H_2, and 0.234 Ω cm^2 in CO at 850 °C, respectively, which further suggested the slower kinetics of CO electro-oxidation.

The durability of cell with SFMN-GDC anode when fueled by syngas ($CO:H_2$=1:1) was further tested under constant current for various durations ranging from tens of hours up to 210 hs between 850 and 750 °C, as shown in Fig. 6. No significant degradation in performance was found even under OCV condition, suggesting that SFMN-GDC has excellent coking tolerance.

3.5 Cell Performance in CH_4

Finally, we evaluated the electro-catalytic activity of the SFMN-GDC when fueled by CH_4 (with addition of only 3% H_2O). Shown in Fig.7a are the I-V-P curves of cells with a configuration of SFMN-GDC ‖ GDC/YSZ/GDC ‖ LSCF, using air as oxidant and humidified CH_4 (3% H_2O) as fuel at 750-850 °C. The peak power densities of the cell are 392, 267 and 161 mW cm^{-2} at temperatures of 850, 800 and 750 °C respectively, the polarization resistance value of the cell is only 0.27, 0.44, and 0.75 Ω cm^2 at 850, 800 and 750 °C, respectively, as shown in Fig. 7b, suggesting that SFMN-GDC have good catalytic activity to methane oxidation. This agrees well with previous studies that ceria-based oxide promotes hydrocarbon oxidation [26]. Firstly, ceria-based oxide becomes a mixed conductor in the reducing atmosphere, potentially expanding the reaction zone beyond three-phase boundaries. Secondly, ceria-based oxide has high ionic conductivity, facilitating the transport of oxygen ions within the anode. Thirdly, ceria-based oxide shows an excellent oxygen storage capability (OSC), which can be further enhance by addition of SFMN. The enhanced OSC may further increase methane oxidation rates.

Fig. 8a presented the short-term stability of the SFMN-GDC ‖ GDC/YSZ/GDC ‖ LSCF cell

under different discharge current densities at 800 °C when fueled with humidified CH_4 (3% H_2O). It has been reported that cells can maintain better stability under high current densities in hydrocarbons based fuels like CH_4 [27]. However, in this work, no obvious degradation was observed at the current density from 0.1 A cm^{-2} to 0.25 A cm^{-2}. Furthermore, the stability of the cell at higher or lower temperature (850 °C and 750 °C) has also been evaluated for several hundred hours, as shown in Fig. 8a. All these results demonstrated that SFMN-GDC have better coking tolerance.

After the durability test in CH_4, the cell was disassembled, and the microstructures of the porous SFMN-GDC anode were examined, as shown in Fig.8b. In general, carbon deposition can occur by methane pyrolysis, $CH_4 \rightarrow C + 2H_2$. A significant result from the cell tests was the absence of carbon deposition. However, the SEM microstructures were also examined for of the porous SFMN-GDC anodes after measurements in CH_4 for 600 hs and in syngas for 210 hs, as shown in the Fig.8b. Nearly no carbon or carbon fibers were detected at the anode side, indicating carbon deposition may be suppressed by reaction between oxygen ions and carbon at the anode during SOFC operation, and suggested the relatively good coking resistance of the SFMN-GDC electrode.

4. Conclusions

In this work, performance and stability of single cells with a configuration of SFMN-GDC ‖ GDC/YSZ/GDC ‖ LSCF were evaluated when fueled by H_2, syngas and CH_4, humidified by 3% H_2O, respectively. Compared with the SFMN anode, SFMN-GDC anode showed much higher activity and better stability when fueled by syngas and methane. In situ exsolved Ni-Fe alloy nanoparticles functioned as a key factor for the anode performance enhancement, while the addition of GDC also promoted hydrocarbon oxidation, suggesting that the SFMN-GDC composite anode is

a good candidate SOFCs anode for direct utilization of hydrocarbons.

Acknowledgment

Financial supports from the National Key R&D Program of China (2017YFB0601904)，Foundation of Beijing Municipal Science and Technology Project (Z181100005118008), the Yueqi Young Scholar Project (CUMTB) and the U.S. National Science Foundation (1832809) are greatly appreciated.

References

[1]. Park S, Vohs JM, Gorte RJ. Direct oxidation of hydrocarbons in a solid oxide fuel cell. Nature 2000;404:265-7. https://doi.org/10.1038/35005040.

[2]. Qin HY, Zhu ZG, Liu QH, Jing YF, Raza R, Imran S, Singh M, Abbas G, Zhu B. Direct Biofuel Low-Temperature Solid Oxide Fuel Cells. Energy & Environmental Science 2011; 4(4):1273-1276. https://doi.org/10.1039/C0EE00420K.

[3]. Sun CW, Stimming U. Review Recent anode advances in solid oxide fuel cells. Journal of Power Sources 2007;171:247-260. https://doi.org/10.1016/j.jpowsour.2007.06.086.

[4]. Aslannejad H, Barelli L, Babaie A, Bozorgmehri S. Effect of air addition to methane on performance stability and coking over NiO–YSZ anodes of SOFC. Applied Energy 2016;177:179-186. https://doi.org/10.1016/j.apenergy.2016.05.127.

[5]. Huang YH, Dass RI, Xing ZL, Goodenough JB. Double perovskites as anode materials for solid-oxide fuel cells. Science 2006;312:254-257. https://doi.org/10.1126/science.1125877.

[6]. Zhu TL, Yang ZB, Han MF. Performance evaluation of solid oxide fuel cell with in-situ

methane reforming. Fuel 2015;161:168-173. https://doi.org/10.1016/j.fuel.2015.08.050.

[7]. Kim JS, Nair VV, Vohs JM, Gorte RJ. A study of the methane tolerance of LSCM-YSZ composite anodes with Pt, Ni, Pd and ceria catalysts. Scripta Materialia 2011;65:90-95. https://doi.org/10.1016/j.scriptamat.2010.06.016.

[8]. Tao SW, Irvine JTS. A redox-stable efficient anode for solid-oxide fuel cells. Nature Materials 2003;2:320-323. https://doi.org/10.1038/nmat871.

[9]. Ma Q, Tietz F. Comparison of Y and La-substituted $SrTiO_3$ as the anode materials for SOFCs. Solid State Ionics 2012;225:108-112. https://doi.org/10.1016/j.ssi.2012.03.048.

[10]. Huang YH, Dass RI, Xing ZL, Goodenough JB. Double perovskites as anode materials for solid-oxide fuel cells. Science 2006;312:254-257. https://doi.org/10.1126/science.1125877.

[11]. Liu Q, Dong XH, Xiao GL, Zhao F, Chen FL. A Novel Electrode Material for Symmetrical SOFCs. Advanced Materials 2010;22:5478-5482. https://doi.org/10.1002/adma.201001044.

[12]. Xiao GL, Chen FL. Ni modified ceramic anodes for direct-methane solid oxide fuel cells. Electrochemistry Communications 2011;13:57-59. https://doi.org/10.1016/j.elecom.2010.11.012.

[13]. Sariboga V, Oksuzomer MAF. Cu-CeO_2 anodes for solid oxide fuel cells: Determination of infiltration characteristics. Journal of alloys and compounds 2016;688:323-331. https://doi.org/10.1016/j.jallcom.2016.07.217.

[14] Dragos Neagu, Tae-Sik Oh, David N. Miller, Herv´e Me´nard, Syed M. Bukhari, Stephen R. Gamble, Raymond J. Gorte, John M. Vohs & John T.S. Irvine, Nano-socketed nickel particles with enhanced coking resistance grown in situ by redox exsolution, Nature Communications, 2015; 6:8120. https://doi.org/10.1038/ncomms9120

[15]. Yang CH, Yang ZB, Jin C, Xiao GL, Chen FL, Han MF. Sulfur-tolerant redox-reversible anode

material for direct hydrocarbon solid oxide fuel cells. Advanced Materials 2012;24:1439-1443. https://doi.org/10.1002/adma.201104852.

[16]. Yang ZB, Xu N, Han MF, Chen FL. Performance evaluation of $La_{0.4}Sr_{0.6}Co_{0.2}Fe_{0.7}Nb_{0.1}O_{3-\delta}$ as both anode and cathode material in solid oxide fuel cells. International Journal of Hydrogen Energy 2014;39:7402-7406. https://doi.org/10.1016/j.ijhydene.2014.01.009.

[17]. Du ZH, Zhao HL, Yi S, Xia Q, Gong Y, et al. High-Performance Anode Material $Sr_2FeMo_{0.65}Ni_{0.35}O_{6-\delta}$ with In Situ Exsolved Nanoparticle Catalyst. ACS NANO 2016;10:8660-8669. https://doi.org/10.1021/acsnano.6b03979.

[18]. Steil MC, Nobrega SD, Georges S, Gelin P, Uhlenbruck S, Fonseca FC. Durable direct ethanol anode-supported solid oxide fuel cell. Applied Energy 2017;199:180-186. https://doi.org/10.1016/j.apenergy.2017.04.086.

[19]. Dai NN, Feng J, Wang ZH, Jiang TZ, Sun W, Qiao JS, Sun KN. Synthesis and characterization of B-site Ni-doped perovskites $Sr_2Fe_{1.5-x}Ni_xMo_{0.5}O_{6-\delta}$ (x = 0, 0.05, 0.1, 0.2, 0.4) as cathodes for SOFCs. Journal of Materials Chemistry A, 2013;1:14147-14153. https://doi.org/ 10.1039/c3ta13607h.

[20] L. dos Santos-Gómez, L. León-Reina, J.M. Porras-Vázquez, E.R. Losilla, D. Marrero-López. Chemical stability and compatibility of double perovskite anode materials for SOFCs. Solid State Ionics, 2013;239: 1-7.

[21]. Zhu TL, Fowler DE, Poeppelmeier KR, Han MF, Barnett SA. Hydrogen Oxidation Mechanisms on Perovskite Solid Oxide Fuel Cell Anodes. Journal of The Electrochemical Society 2016;163 (8):F952-F961. https://doi.org/10.1149/2.1321608jes.

[22]. Cho S, Fowler DE, Miller EC, Cronin JS, Poeppelmeier KR, Barnett SA. Fe-substituted

$SrTiO_{3-\delta}$-$Ce_{0.9}Gd_{0.1}O_2$ composite anodes for solid oxide fuel cells. Energy & Environmental Science 2013;6:1850-1857. https://doi.org/10.1039/c3ee23791e.

[23]. Yoo KB, Choi GM. LST-GDC composite anode on $LaGaO_3$-based solid oxide fuel cell. Solid State Ionics 2011;192:515-518. https://doi.org/10.1016/j.ssi.2010.06.048.

[24]. Sun XF, Wang SR, Wang ZR, Ye XF, Wen TL, Huang FQ. Anode performance of LST-xCeO_2 for solid oxide fuel cells. Journal of Power Sources 2008;183:114-117. https://doi.org/10.1016/j.jpowsour.2008.05.007.

[25]. Xu N, Zhu TL, Yang ZB, Han MF. Fabrication and optimization of $La_{0.4}Sr_{0.6}Co_{0.2}Fe_{0.7}Nb_{0.1}O_{3-\delta}$ electrode for symmetric solid oxide fuel cell with zirconia based electrolyte. Journal of Materials Science & Technology 2017;33:1329-1333. https://doi.org/10.1016/j.jmst.2017.03.012

[26] Chen Y, Zhang YX, Lin Y, Yang ZB, Su D, Han MF, Chen FL. Direct-methane solid oxide fuel cells with hierarchically porous Ni-based anode deposited with nanocatalyst layer. Nano Energy 2014;10:1-9. https://doi.org/10.1016/j.nanoen.2014.08.016

[27] Atkinson A, Barnett SA, Gorte RJ, Irvine JTS, McEvoy AJ, Mogensen M, Singhal SC, Vohs J. Advanced anodes for high-temperature fuel cells. Nature Materials 2004;3:17-27. https://doi.org/10.1038/nmat1040.

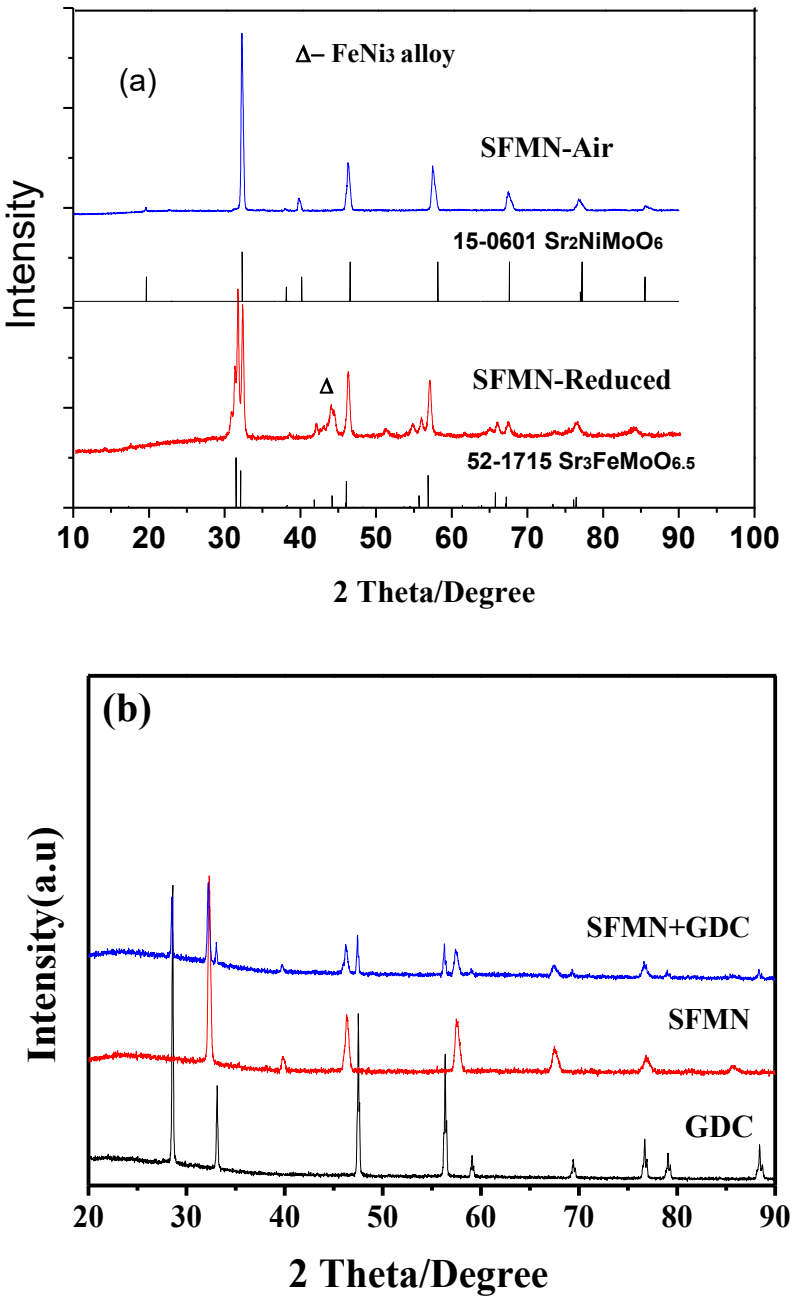

Fig.1. (a) Room-temperature XRD patterns of as-prepared SFMN powders and after reduction in pure H_2 for 10 h; (b) XRD patterns of SFMN, GDC and SFMN-GDC (1:1) powders.

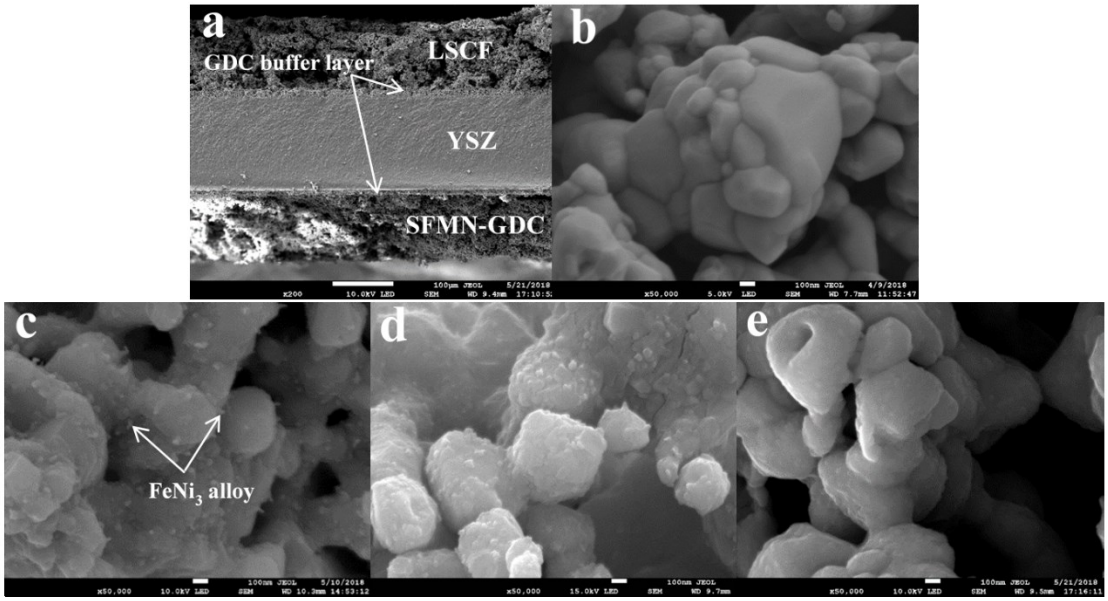

Fig.2. Microstructure characterization: (a) SEM images of the SFMN-GDC|GDC/YSZ/GDC|LSCF cell; (b) SFMN-GDC anode before reduction, (c) SFMN-GDC after reduction; (d) SFMN-GDC after three redox cycles; and (e) SFM-GDC anode after reduction.

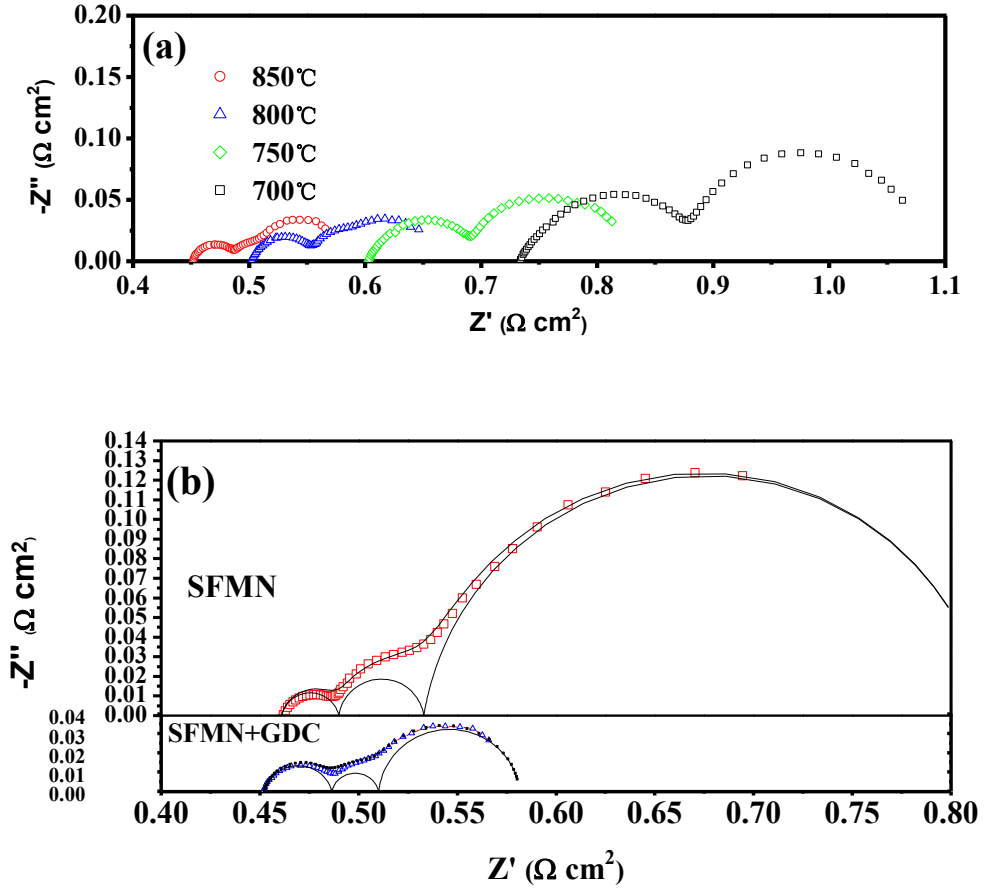

Fig.3. (a) Impedance spectra for the SFMN-GDC‖GDC/YSZ/GDC‖LSCF cell and (b) Example fits to the EIS data of SFMN-GDC and SFMN anode cell tested at 850 ºC at open-circuit voltage.

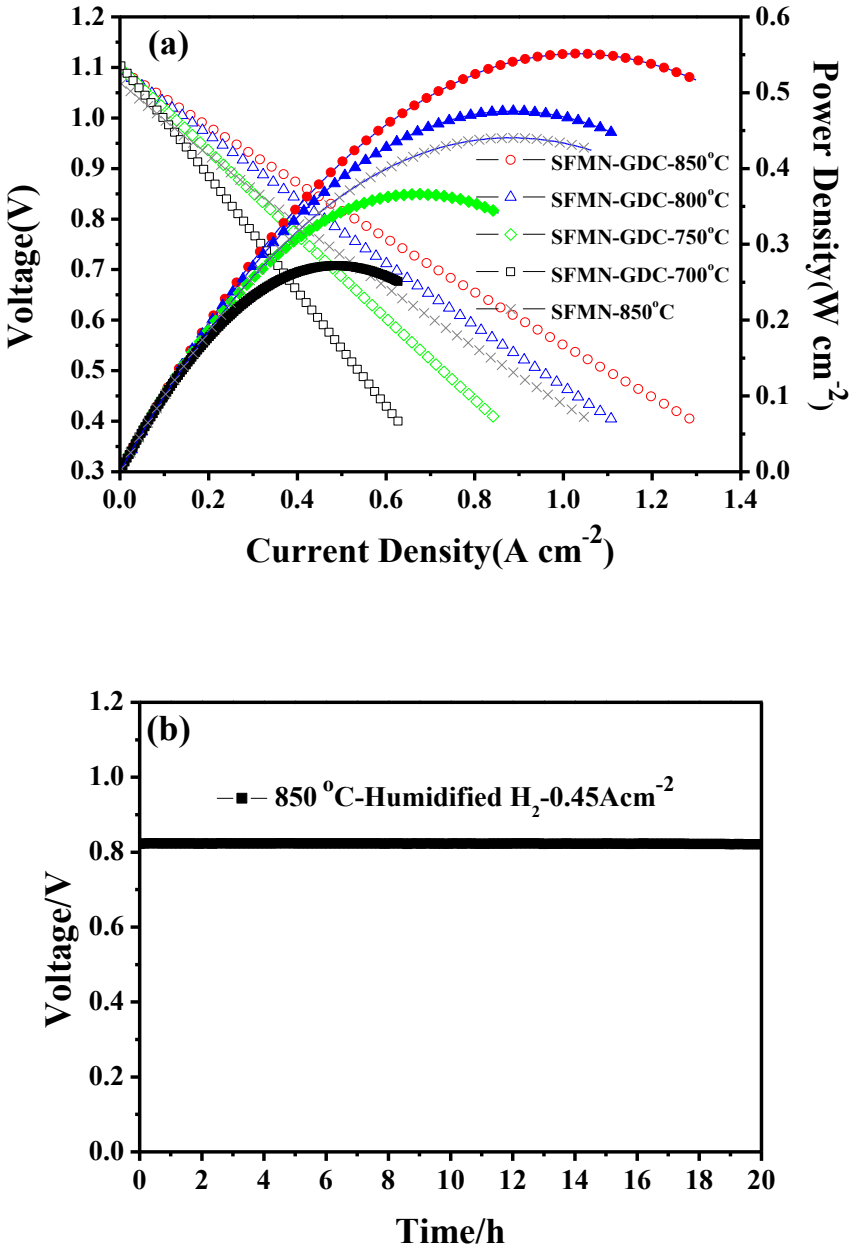

Fig. 4. (a) Voltage-current curves and (b) Stability test under constant current of 0.45 A cm^{-2} at 850 °C using H_2 for the SFMN-GDC‖GDC/YSZ/GDC‖LSCF cell.

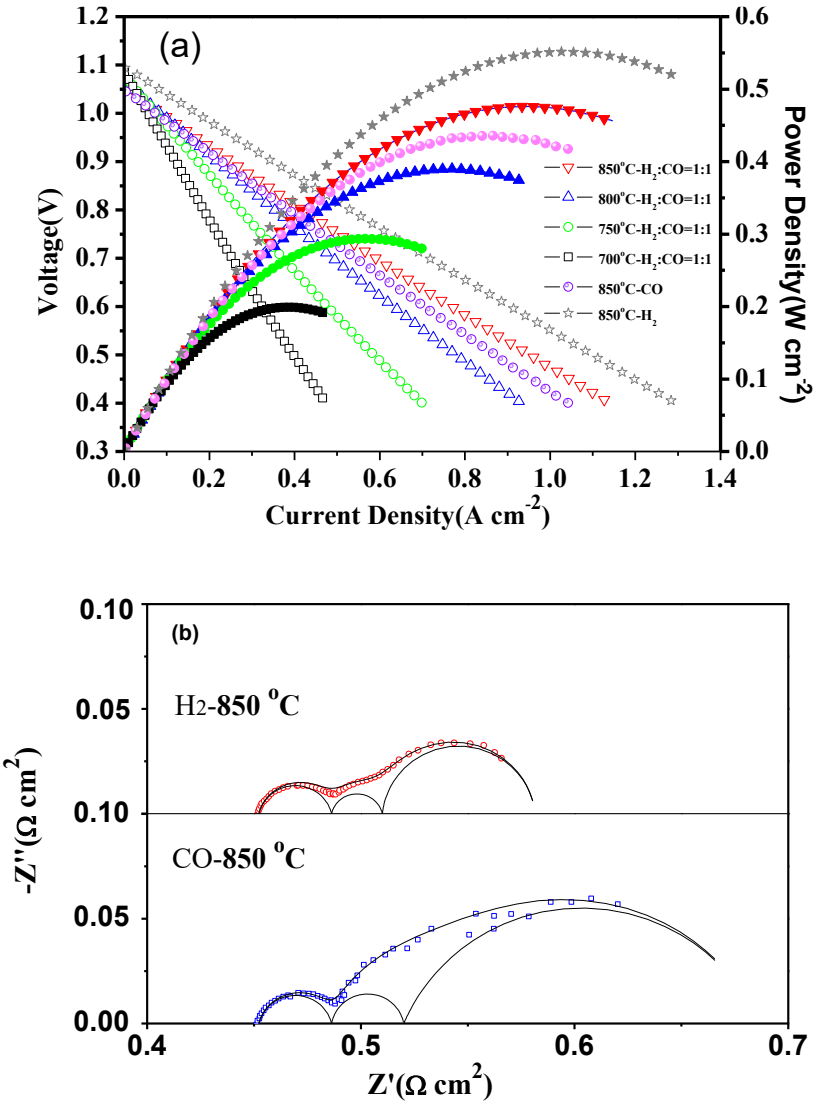

Fig.5. (a) Voltage-current curves and (b) impedance spectra of SFMN-GDC‖GDC/YSZ/GDC‖LSCF cell measured at different temperatures in CO-H_2.

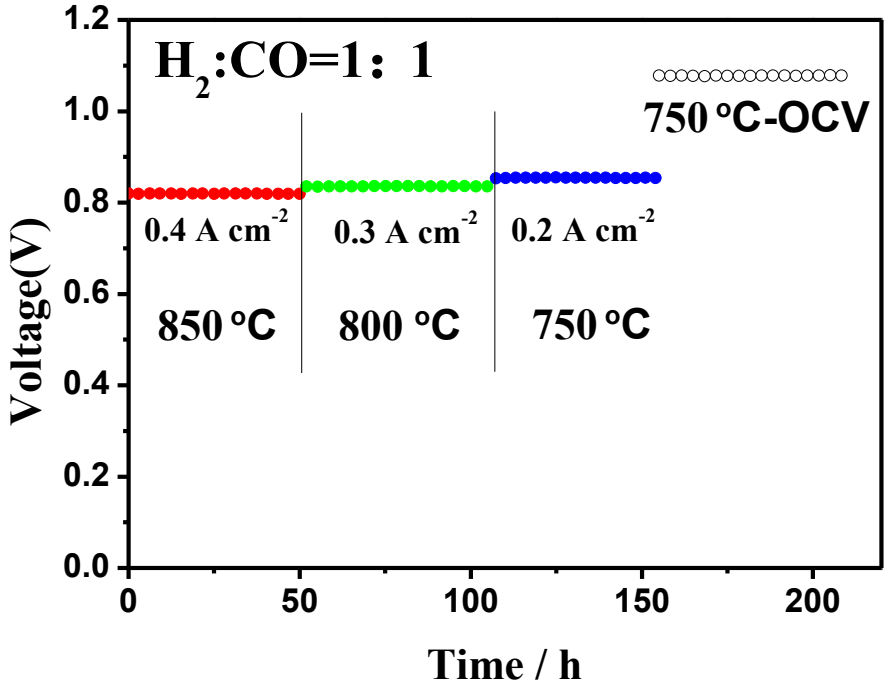

Fig. 6. Stability test under different current densities and different temperature using CO-H_2 for the SFMN-GDC‖GDC/YSZ/GDC‖LSCF cell.

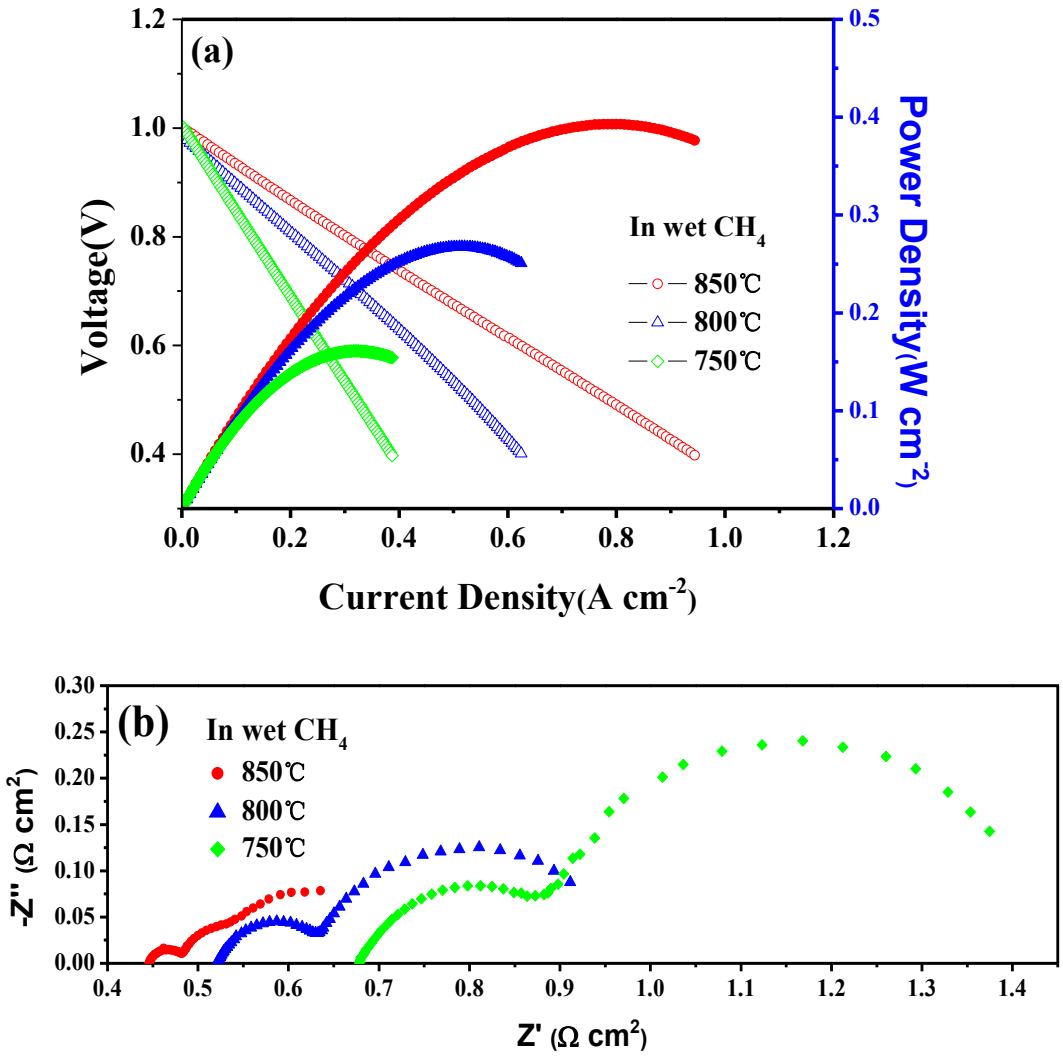

Fig.7. (a) Voltage-current curves and (b) impedance spectra of SFMN-GDC|GDC/YSZ/GDC|LSCF cell measured at different temperatures in humidified CH_4 (3% H_2O).

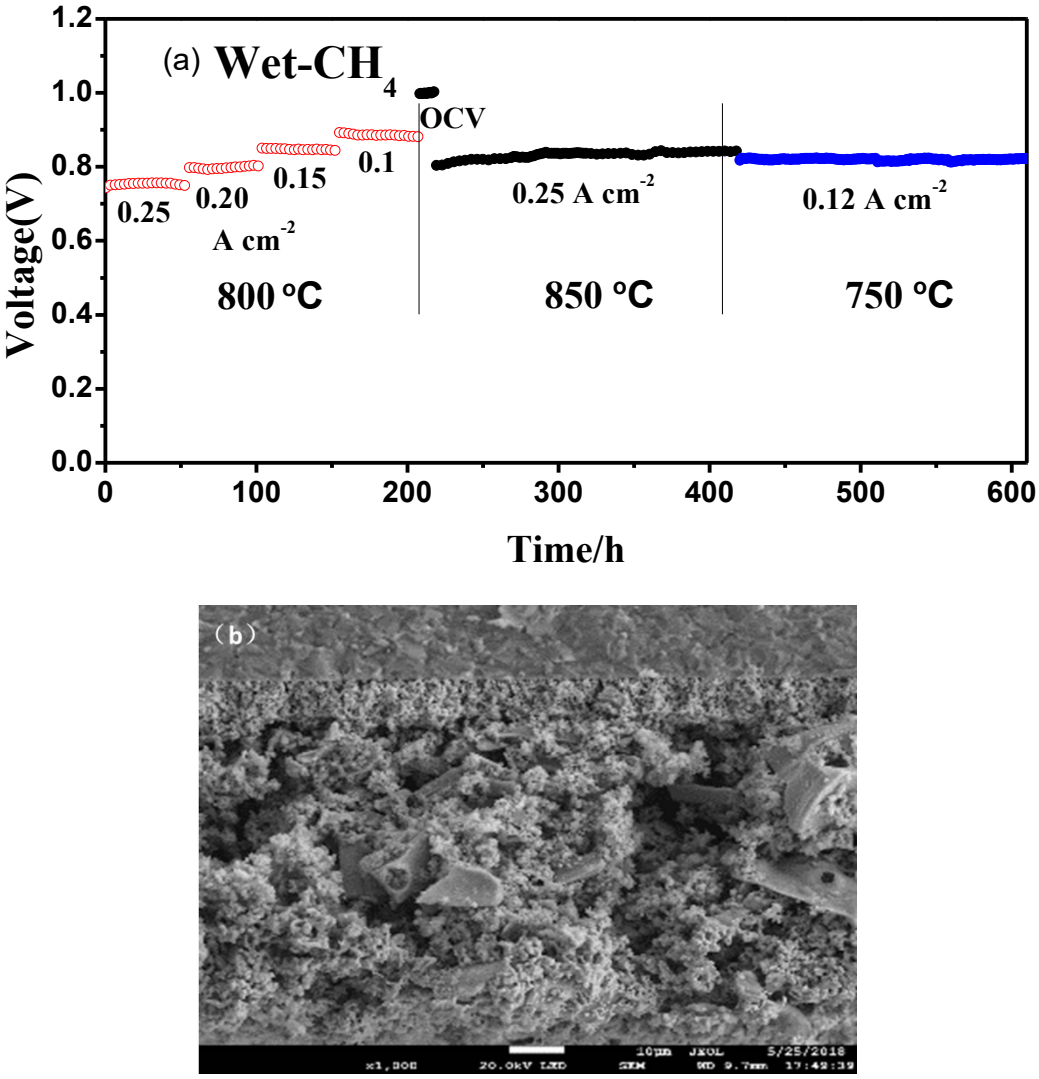

Fig.8. (a) Voltage versus operation time of the single cell fuelled with humidified CH_4 (3% H_2O) at different current densities and different temperature. (b) Cross-sectional SEM images of the cells with SFMN-GDC anodes after H_2, syngas and CH_4 test.